AIAA JOURNAL
Vol. 60, No. 2, February 2022

Computational Investigation of Multirotor Interactional Aerodynamics with Hub Lateral and Longitudinal Canting

Richard Healy* and Farhan Gandhi†
Rensselaer Polytechnic Institute, Troy, New York 12180
and
Mihir Mistry‡
The Boeing Company, Ridley Park, Pennsylvania 19078

https://doi.org/10.2514/1.J060530

This study investigates the interactional aerodynamics for laterally and longitudinally canted two-rotor systems with a front rotor and an aft rotor aligned with the flow. The 5.5-ft-diameter, three-bladed fixed-pitched rotors are simulated using computational fluid dynamics at a targeted 5 lb/ft^2 disk loading and 30 kt edgewise freestream. Simulations are performed using the commercial Navier—Stokes solver AcuSolve with a detached eddy simulation model. In addition to an uncanted case, two laterally canted cases (10° advancing sides up and 10° advancing sides down) as well as two longitudinally canted cases (10° inward and 10° outward) are simulated. Aft rotor performance is compared to isolated rotors operating at the same revolutions per minute, speed, and shaft tilt angle in order to quantify the effect of rotor–rotor aerodynamic interaction. For all configurations, the aft rotors experience a lift deficit at the front of the rotor disk, which also results in a nose-down pitching moment relative to an isolated rotor. The lift deficit for the uncanted rotor was around 15%. Lateral canting only slightly increases the lift deficit (to 16–18%) but also produces 28–38% change in roll moments. Change in aft rotor nose-up pitching moments for the uncanted and laterally canted rotors were in the 55–64% range. Longitudinal canting produces larger changes in the magnitude of the lift deficit and pitching moment, but has minimal effect on roll moments. In particular, canting inward results in a lift deficit as high as 21% and a 94% change in pitching moment. Canting outward, on the other hand, reduces the aft rotor lift deficit to 11% and the pitching moment change to 19%. The paper explains the changes in the flowfield and the underlying physics for the different cases in detail.

I. Introduction

ALTHOUGH hobbyists, recreational users, and enterprising videographers have been operating small multicopters for a long time, the last few years have seen a tremendous interest in larger multirotor electric (eVTOL) vertical takeoff and landing (VTOL) aircraft for urban air mobility, commercial package delivery, cargo, and military/law-enforcement applications, among others. The current batteries powering most of these eVTOL aircraft exhibit very low energy density relative to hydrocarbon fuels used by larger conventional VTOL aircraft. With this limitation, it is especially important to maximize the aerodynamic performance of eVTOL aircraft in order to realize practical payload capacity, endurance, and range. Because these metrics were not as important to recreational users of smaller multicopters, they have not previously received much consideration. One area that requires particular attention is the understanding of the interactional aerodynamic effects of multiple rotors operating in close proximity and their impact on aerodynamic performance.

A number of recent studies have used high-fidelity computational fluid dynamics (CFD) to simulate and understand the complex flows associated with interactional aerodynamics of rotors operating in close proximity. Researchers at the NASA Advanced Supercomputing Division have used CFD to simulate large- and small-scale quadcopters in hover and forward flight. Yoon et al. [1,2] investigated the effects of turbulence modeling and rotor separation on an XV-15 derivative quadcopter in hover, and determined that decreasing the separation between rotors reduces the thrust generated, by up to 4%. At the smaller scale, Yoon et al. simulated the DJI Phantom 3 and straight up endurance (SUI) Endurance quadcopters [3], and determined that at 10 m/s cruise, the rear rotors produced up to a 28% thrust deficit than when operating in isolation. Other work by Ventura Diaz and Yoon [4] found that vertical rotor separation on a quadcopter via over/under mounting influenced rotor interaction in cruise.

Misiorowski, Gandhi, and Oberai, at Rensselaer Polytechnic Institute's (RPI's) Center for Mobility with Vertical Lift (MOVE), also used high-fidelity CFD to simulate quadcopters operating in cruise in the plus and cross configurations [5], and provided physical insights into the difference in interactional aerodynamics for the two configurations. Notably, they reported that in the plus configuration, the side rotors operating in the upwash of the front rotor wake showed power benefits. This phenomenon was recently corroborated by another study from researchers at the Delft University of Technology and Netherlands Defense Academy [6]. Also from RPI, Healy et al. [7] systematically examined the effects of vertical and longitudinal rotor spacing on interactional aerodynamics of an in-line two-rotor assembly in edgewise flight. Over the last few years, NASA has developed a reconfigurable Multirotor Testbed (MTB), where the relative positions and orientations of various rotors can be changed. Experiments conducted on this testbed in the 7 × 10 ft wind tunnel at Ames Research Center [8] have shown reductions in aft rotor thrust previously reported in computational studies. Researchers from NASA have also compared multirotor aerodynamic interaction effect simulations using a midfidelity CFD analysis [9] to the MTB test results.

Whereas the preceding studies have simulated multirotor configurations with uncanted rotors, many modern eVTOL designs are incorporating canted rotors, where the axis of rotation is inclined from the vertical (Fig. 1), in an effort to realize benefits that include improved yaw authority [10,11].[§,¶] As the size of multirotor eVTOL vehicles has grown, so too has the size of the rotors used on these vehicles. However, when rotor radius exceeds approximately 2 ft, the handling

Received 8 January 2021; revision received 21 June 2021; accepted for publication 21 July 2021; published online 28 September 2021.

*Ph.D. Student for the Center for Mobility with Vertical Lift (MOVE), 110 8th Street. Student Member AIAA.
†Rosalind and John J. Redfern Jr. Chair in Engineering and Director for the Center for Mobility with Vertical Lift (MOVE), 110 8th Street. Fellow AIAA.
‡Guidance, Navigation and Control Engineer, 1 S. Stewart Ave.

§"PAV–Passenger Air Vehicle," Aurora Flight Sciences, May 2019, https://www.aurora.aero/pav-evtol-passenger-air-vehicle.
¶"Wisk Cora Aircraft," Wisk, May 2021, https://wisk.aero/aircraft/.

qualities of variable RPM controlled multicopters degrades [12–14] for moderate motor sizing. Rotor canting can significantly improve yaw control authority by using the thrust generated by the rotors to produce aircraft yaw moments [11,15]. However, the effect of rotor canting on aerodynamic performance, especially on the interactional aerodynamics for multirotor assemblies, is largely unknown. The present study looks to conduct simulations to examine the interactional aerodynamic effects in edgewise flight for a large urban-air-mobility-scale in-line two-rotor unit incorporating differential lateral and longitudinal rotor cant. The CFD simulations use the commercial Navier–Stokes solver AcuSolve [16], previously used by the authors in Refs. [5,7]. This study also focuses on examining the underlying physical phenomena behind the differences in behavior for the different canted cases.

II. Analysis

Two in-line fixed-pitch rotors in forward flight are simulated using CFD. The front rotor spins clockwise and the aft rotor spins counterclockwise at the same rotational speed. Rotor hubs are positioned in-line with the freestream, as seen on many large eVTOLs such as the Aurora passenger air vehicle (PAV) Fig. 1 [17] or the Wisk Cora (see footnote ¶). In particular, the rotor hubs are positioned with 2.5 R longitudinal separation, and no vertical separation. However, although the position of the rotors is held constant, the relative shaft tilt angle, or cant of each rotor, is varied. For lateral canting, both rotors are set at zero pitch attitude relative to the flow, and are tilted in the roll direction. Three configurations are shown in Fig. 2: uncanted, 10° cant with the advancing sides up, and 10° cant with the advancing sides down. In contrast, for longitudinal canting, both rotors are tilted in opposite directions along the pitch axis. Figure 3 compares uncanted, 10° cant inward, and 10° cant outward cases.

The rotors used have a 5.5 ft diameter, with specifications detailed in Table 1. A CAD image of the rotor is shown in Fig. 4. The Rensselaer Multirotor Analysis Code [18], based on blade element theory with 3 × 4 finite-state Peters–He inflow representation is used to evaluate an appropriate root pitch and RPM for a target 5 $\mathrm{lb/ft^2}$ disk loading in hover. A 22° root pitch and 1600 RPM is found to provide sufficiently low power and hover tip Mach number. CFD simulations are performed at 30 kts forward speed, which represents a $\mu = 0.1$ advance ratio.

Table 1 Rotor parameters

Parameter	Specification
Diameter	5.5 ft
Number of blades	3
Solidity	0.076
Root cutout	0.2 R
Airfoil	NACA 23012
Twist	−10°
Planform	Rectangular
Chord	6.56 in
Root pitch	22°
RPM	1600 RPM
Hover Tip Mach No.	0.41

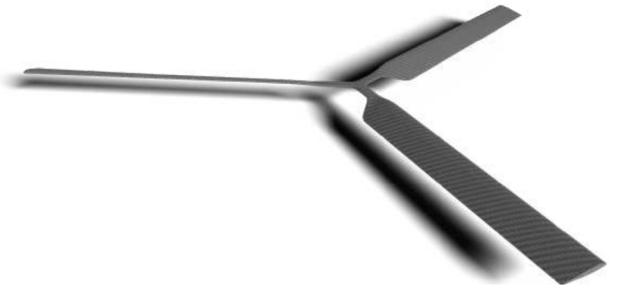

Fig. 4 Rotor CAD.

All simulations are conducted using the commercial Navier–Stokes solver AcuSolve, which uses a stabilized second-order upwind finite element method, and has been validated for external aerodynamic flows [16,19]. AcuSolve simulation results for an SUI endurance rotor in hover were previously shown to compare well against experiment in Ref. [5], where thrust at two different rotor speeds in hover matched experiment within 3%. Other studies using

Fig. 1 Laterally canted rotors on the Boeing PAV. Reprinted with permission from the Vertical Flight Society [17].

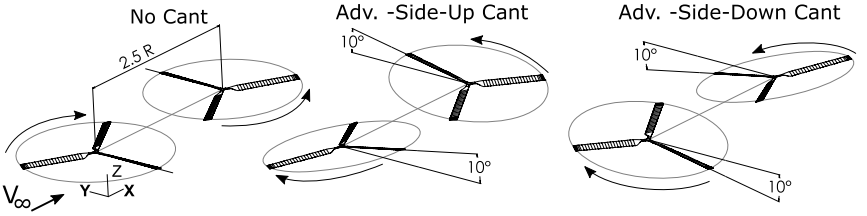

Fig. 2 Two-rotor system for uncanted, advancing-side-up, and advancing-side-down cant cases.

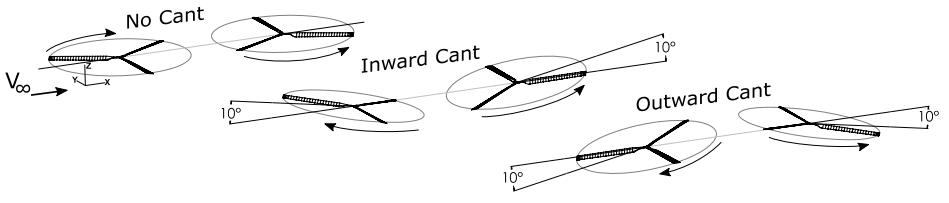

Fig. 3 Two-rotor system for uncanted, canted inward, and canted outward cases.

AcuSolve to simulate rotor aerodynamics have previously been published in peer-reviewed journals such as the AIAA Journal [5,20], as well as the Journal of the American Helicopter Society [21]. For a two-rotor unit, the computational domain is shown in Fig. 5. The nonrotating volume is a rectangular prism with sides at least 25 rotor radii away from the front rotor hub. The front and top boundaries are set to the freestream velocity, whereas the sides, bottom, and back are set to outflow with backflow conditions enabled, which allows for flow in either direction across the boundary with zero pressure offset. Around each rotor is a cylindrical rotating volume with radius 1.06 rotor radii and extending over two chord lengths above and below the rotor plane. Each surface of the cylindrical rotating volumes has a sliding mesh interface that passes information to and from the nonrotating volume that comprises the remainder of the computational domain.

The domain is discretized using an entirely unstructured, tetrahedral mesh. On each blade, the surface mesh is set to ensure 200 elements around the airfoil contour, with refinement along the leading and trailing edges (0–10% and 90–100% chord, respectively). A portion of the blade surface mesh is shown in Fig. 6. The boundary layer in the wall-normal direction is highly resolved, with the first element height set to ensure a $y+ < 1$. The boundary layer is grown until the last layer size is within 80% of the local off-body element size (approximately 43 layers). A clipped slice of the mesh shows the boundary layer in Fig. 6. Around the rotors (1 R above and below), a wake refinement region is defined in which the element size is prescribed as 1/4 chord and applies to both the rotating and nonrotating volumes. Below and downstream of the rotor plane, a second refinement region is prescribed with elements 1/2 chord in size. This second refinement region is skewed back in order to capture the rotor wake as it convects downstream (Fig. 7). The entire computational domain is comprised of 120 million elements, with 48 million in each rotating volume, and 24 million in the surrounding nonrotating volume. A detailed mesh refinement study was performed in which the surface mesh size, edge refinement, boundary layer, and wake refinement were doubled independently. For the mesh used in the simulations, the thrust and torque changed by less than 1.5% and 2%, respectively, when compared to the finer meshes.

A detached eddy simulation (DES) is used with the Spalart–Allmarus turbulence model for all simulations. Each case is initially run using time steps corresponding to 10° of rotation for at least 40 revolutions in order to reduce the computational cost of rotor wake development. These initial 10° time steps are possible without numerical divergence due to the stability afforded by the streamline upwind Petrov–Galerkin stabilized finite element method and generalized α implicit time integration method. The latter method was designed to suppress high-frequency disturbances and allow solution stability with Courant–Friedrichs–Lewy number greater than 1 [22,23]. Following the revolutions simulated with 10° time steps, at least three additional revolutions are simulated with time steps corresponding to 1°. Three revolutions is sufficient time to allow flow at the front rotor to travel downstream of the aft rotor. A maximum of 15 subiterations are allowed at 1° time steps, providing two orders of magnitude residual drop at each time step. All runs are performed on 512 2.6 GHz Intel Xeon E5-2650 processors, part of the Center for Computational Innovations at Rensselaer Polytechnic Institute.

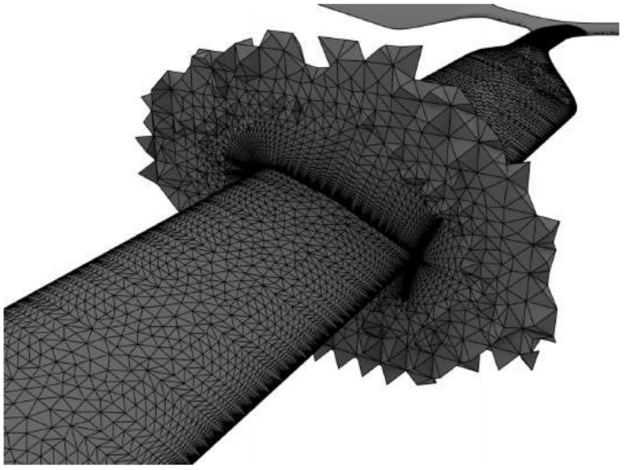

Fig. 6 Blade surface and boundary-layer mesh at midspan.

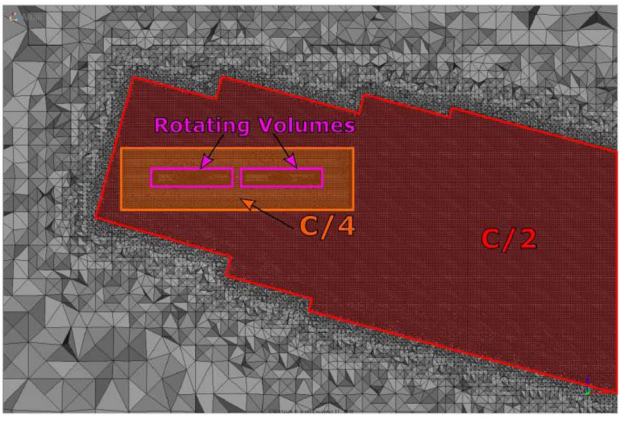

Fig. 7 Cross section of wake mesh refinement, with rotor tip paths highlighted in pink.

III. Results

A. Uncanted Rotor Performance

An isolated counterclockwise rotor in 30 kt nose-level flight is simulated at 1600 RPM. This condition represents how the aft rotor

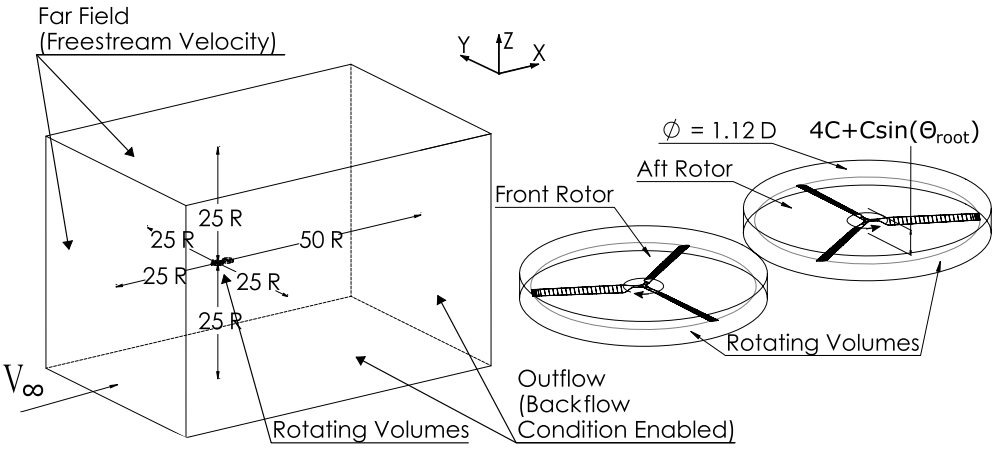

Fig. 5 Diagram of the computational domain.

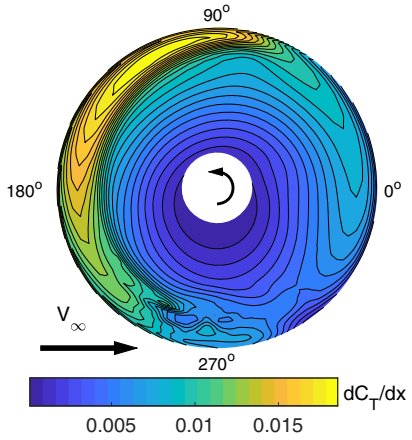

Fig. 8 Sectional thrust coefficient, dCt/dx, for isolated rotor.

in an uncanted two-rotor system would perform in the absence of a front rotor. Figure 8 shows the sectional thrust coefficient (dC_T/dx) for the isolated rotor with flow moving from left to right. Relatively higher thrust is produced at the front of the rotor disk on the advancing side (second quadrant). This observation is consistent with that seen in Ref. [24] and is caused by higher dynamic pressure on the advancing side of the rotor, in conjunction with longitudinal inflow variation [25].

An uncanted two rotor system is first simulated to identify the interactional aerodynamic effects. Figure 9 shows the sectional thrust coefficient (dC_T/dx) for the front and aft rotors, again in 30 kt nose-level flight at 1600 RPM. The front rotor for this case shows nearly identical performance characteristics to an isolated clockwise rotor, indicating the aft rotor in this system has little effect on the front rotor. In contrast, the aft rotor exhibits a smaller area of high thrust, which lies farther back on the rotor disk (around $\psi = 90°$) when compared to the isolated rotor case in Fig. 8 (high lift centered around $\psi = 110°$, and extending past $\psi = 150°$). By comparing isolated and aft rotor loads in this way, the effect of interactional aerodynamics can be extracted.

B. Uncanted/Laterally Canted Front Rotor Wake Aerodynamics

The difference in aft rotor thrust distribution compared to the isolated case can be explained through investigation of the front rotor wake convection. Figure 10 shows induced vertical (Z) velocity averaged over one revolution on a plane cutting through the aft rotor disk (no aft rotor actually simulated). Isosurfaces of Q-criterion colored by x-vorticity are also shown. In the region between the advancing and retreating side rollup vortices, strong downwash is observed on the plane cutting through the location of the aft rotor disk (outlined in magenta). Outside the rollup vortices, upwash is induced. The advancing side vortex rollup is observed to convect downward faster than the retreating side vortex rollup due to greater thrust production on the advancing side. Figure 10 (right) also shows slice A:A as viewed from the rear.

Figure 11 compares slice A:A from Fig. 10 as viewed from the rear for the uncanted as well as the two laterally canted assemblies. Here, the uncanted rotor is seen to lie at the top of the strong downwash region. However, when the rotors are canted with the advancing sides up, the aft rotor's retreating side is positioned closer to the front rotor's advancing side rollup vortex. This close proximity causes the aft rotor's retreating side to interact with areas of higher downwash. On the advancing side, the canted aft rotor is positioned farther away from the front rotor's retreating side rollup vortex, away from the strongest downwash. With the rotors canted with advancing sides down, the reverse is observed. The aft rotor disk's retreating side is positioned relatively farther away from the front rotor's advancing side rollup vortex, out of the downwash. Conversely, its advancing side is positioned in close proximity to the retreating side rollup vortex, moving into the region of strong downwash.

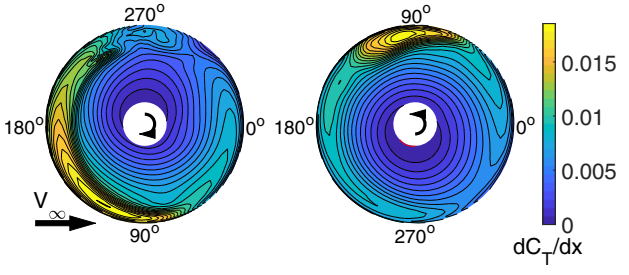

Fig. 9 Sectional thrust coefficient, dCt/dx, for an uncanted two-rotor system.

The effects of rotor cant on downwash and upwash over the entire aft rotor disk can be observed in Fig. 12. This figure shows the rev-averaged velocity normal to the aft rotor plane induced by an isolated front rotor, plotted over the region that would be occupied by an aft rotor (no aft rotor actually simulated). Isosurfaces of Q-criterion are also shown, colored by x-vorticity. For the uncanted case, downwash is strongest at the front of the aft rotor disk, where it is closest to the front rotor wake. Outside of the front rotor wake, upwash is induced. The wake is observed to convect laterally toward the front rotor's advancing side, causing the advancing tip of the aft rotor disk to lie outside of the front rotor wake. As a result, the advancing side of the uncanted disk experiences front rotor wake-induced upwash effect in its tip region.

For the advancing-side-up cant, the greater lateral drift of the front rotor wake relative to the aft rotor puts a larger section of the aft rotor disk's advancing side in the upwash of the front rotor's retreating side rollup vortex. However, as seen in Fig. 11 (middle), the magnitude of this upwash is lower than the uncanted case due to increased vertical separation between the front rotor retreating side rollup vortex and the rear rotor disk's lifted-up advancing side. In Fig. 12 (middle), the retreating side of the aft rotor sees a heavy downwash due to the greater proximity of the aft disk's retreating side to the front rotor's advancing side rollup vortex (Fig. 11).

For the advancing-side-down cant, the lateral drift of the front rotor's wake is in the opposite direction and the aft rotor's retreating tip region does not see downwash (Fig. 12, right). The advancing side's close proximity to the front rotor's retreating side rollup vortex (Fig. 11) produces the strongest downwash over the aft rotor's advancing side (Fig. 12, right).

C. Impact of Lateral Cant on Rotor Thrust and Torque

The downwash and upwash induced on the aft rotor disk seen in Fig. 12 are primary contributors to the differences in thrust distribution on the aft rotor. Figure 13 shows the difference in sectional thrust coefficient between the aft rotor in a two-rotor system and an isolated rotor operating in identical conditions, but in the absence of a front rotor. Thrust for canted rotors is taken normal to the disk plane, thus any reduction in lifting force due to a tilted thrust vector is omitted from this comparison. For the uncanted rotors, downwash on the aft rotor disk leads to a loss in lift. Downwash on a blade section increases the local inflow angle, reducing the blade section's aerodynamic angle of attack, and thus its lift. Aft rotor thrust is also more sensitive to front-rotor-induced downwash in areas where an isolated rotor would produce high thrust. High thrust production is associated with large angle of attack, and a low induced inflow velocity. On portions of the disk where self-induced inflow velocity is low, front-rotor- induced downwash will have a greater relative influence on total inflow velocity. As a result, portions of the isolated rotor disk with high thrust will be more affected by front-rotor-induced downwash than areas with low thrust. For the uncanted aft rotor, a majority of the lift deficit is observed on the front advancing side of the disk, where front-rotor-induced downwash is strong, and isolated rotor thrust production is high. On the advancing side of the disk (around $\psi = 90°$), upwash from the front rotor's retreating side rollup vortex is shown to produce a region of increased lift. Overall, an uncanted aft rotor is found to produce 15% less thrust than an isolated rotor.

The canted case with advancing sides up exhibits a larger region of lift loss on the front retreating side (compare the regions around $\psi =$

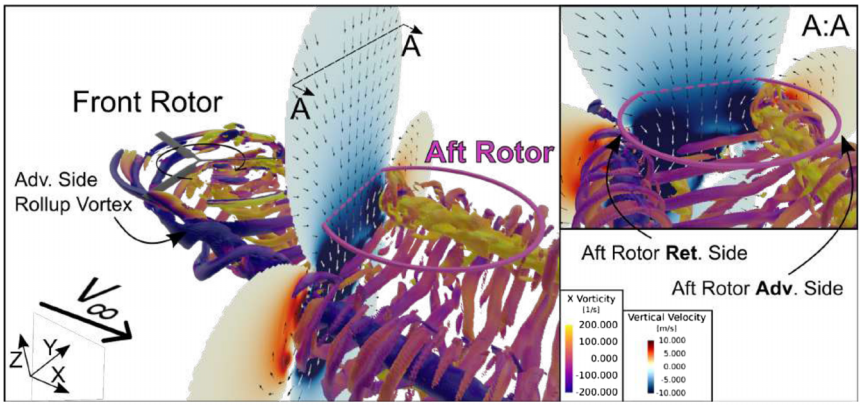

Fig. 10 Velocity induced by the front rotor on three slices intersecting the area occupied by an uncanted aft rotor.

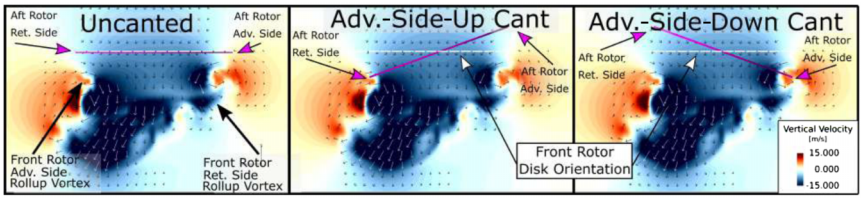

Fig. 11 Slice A:A from Fig. 10 viewed from behind.

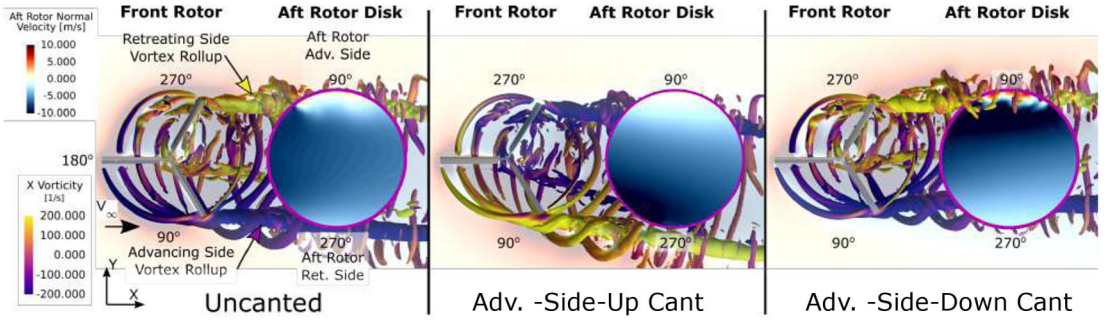

Fig. 12 Front-rotor-induced velocity normal to the aft rotor disk in the region of the aft rotor disk, as well as Q-criterion (7500) of isolated rotor wake colored by vorticity in the freestream direction.

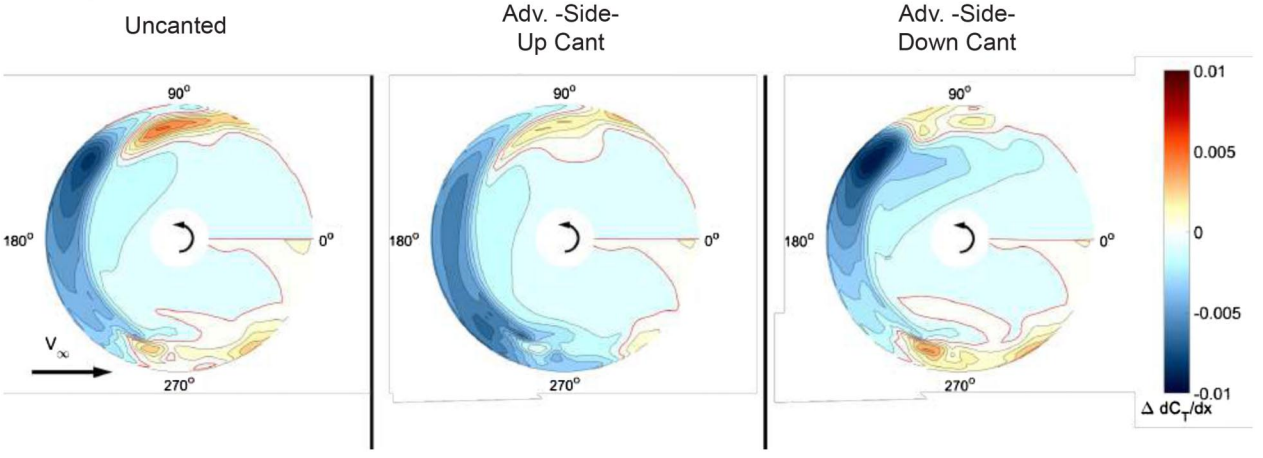

Fig. 13 Sectional thrust coefficient difference, $\Delta dC_T/dx$ (aft rotor thrust minus isolated rotor thrust).

270° between uncanted and advancing-side-up canted cases in Fig. 13). This is a result of the stronger retreating side downwash observed in Fig. 12. Additionally, the peak lift loss observed on the uncanted rotor at $\psi = 120°$ is less dramatic for this canted case, as it sees relatively less downwash in this region. On the advancing side, a larger region of thrust increase, but a lower maximum increase, is observed. This is consistent with the larger region of upwash, but lower upwash magnitude, as seen in Fig. 11. The integrated thrust for the advancing-side-up aft rotor is 17% less than an equivalent rotor in isolation. For rotor cant with advancing sides down, the low downwash on the retreating side of the aft rotor disk (seen in Figs. 11 and 12) results in minimal lift difference over this region ($\psi = 210°$ to

$\psi = 240°$). However, the strong downwash on the advancing side of the disk results in significant loss in lift at about $\psi = 120$ deg. Lift deficit in this region is greater than that seen in the uncanted case due to the canted aft rotor's closer proximity to the front rotor's retreating side rollup vortex (seen in Fig. 11). Overall, the advancing-side-down aft rotor exhibits a 16% thrust deficit compared to an isolated rotor in the same operating conditions.

The changes in interactional aerodynamics brought about by lateral cant also influence the torque on the aft rotor. Figure 14 presents the difference in sectional torque coefficient between the aft rotor in a two-rotor system, and an isolated rotor. For all cases, downwash on the front of the rotor disk leads to an increase in torque in this area. Downwash on a blade element decreases the local angle of attack, tilting the lift vector backward, increasing induced drag. The aft rotor with advancing side up displays a weaker torque penalty on the front advancing side (around $\psi = 90°$ to $\psi = 135°$) compared to the uncanted case. As with lift loss, this reduction in torque penalty corresponds to the lesser downwash observed in this region in Fig. 12. Overall, the advancing-side-up aft rotor requires 2% more torque than an isolated rotor, whereas the uncanted aft rotor requires 7% more. The opposite is true of the advancing-side- down case, where a greater torque penalty compared to the uncanted case is observed around $\psi = 130°$ due to the stronger downwash observed in that region in Fig. 12. In total, however, the advancing-side-down rotor requires 7% greater torque than a rotor in isolation, similar to that of the uncanted system.

For every lateral cant case, a region of significant torque reduction is observed starting at about $\psi = 230°$ on the aft rotors. This feature is a result of blade vortex interaction (BVI) on an isolated rotor in these operating conditions, but not on the aft rotors. Blade vortex interaction on an isolated rotor leads to a localized area of high torque starting at $\psi = 230°$ (Fig. 15). In the two-rotor systems, front-rotor-induced downwash on the aft rotor pushes the aft rotor's tip vortices down and weakens BVI effects. As a result, the presence of a front rotor eliminates the localized area of high torque that was observed on the isolated rotor. With the high-torque region present on an isolated rotor, but not on the aft rotors, Fig. 14 shows localized regions of relative torque reduction at $\psi = 230°$. Integrated changes in torque that have been reported are also affected by the BVI events. When BVI is not observed on the isolated rotor (as with other, high-disk-loading cases that were simulated but have not been included in this paper), the localized regions of torque reduction seen in Fig. 14 are absent. BVI effects aside, a torque increase is broadly observed on the front of the aft rotor disk for all three cases (red regions seen in Fig. 14). Overall, torque penalty for the advancing-side-up case is lower than the uncanted case, but for the advancing-side-down case, it is higher.

D. Longitudinal Cant of an Isolated Rotor

For the two-rotor system considered in this study, longitudinal canting is examined with the rotors either tilting downward toward each other (inward cant) or tilting upward away from each other (outward cant), as shown in Fig. 3. For inward canted rotors, the front rotor is pitched nose-up and the aft rotor is pitched nose-down relative to an uncanted rotor. The reverse is true for outward canted rotors. Figure 16 shows the thrust difference between an isolated rotor pitched 10° nose-down and an uncanted rotor (nose-down minus uncanted). This represents how changing just the relative angle of attack influences a canted rotor's thrust due to the component of the freestream velocity acting downward through the rotor disk. This downwash over the rotor disk leads to a loss in lift, as indicated by the large predominantly blue region in Fig. 16. Overall, the nose-down

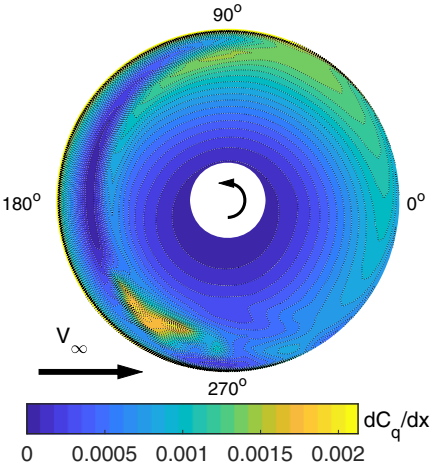

Fig. 15 Sectional torque coefficient, dCq/dx, for isolated rotor.

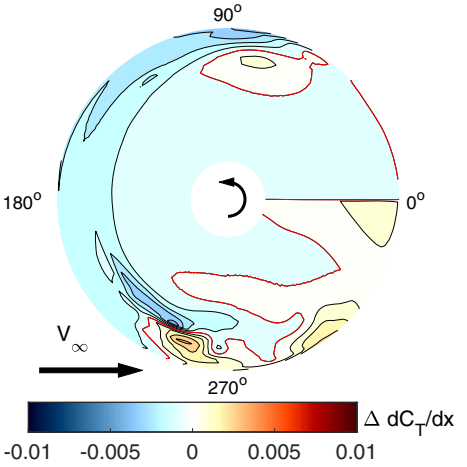

Fig. 16 Sectional thrust coefficient difference, $\Delta dC_t/dx$ (isolated nose-down thrust minus isolated uncanted rotor thrust).

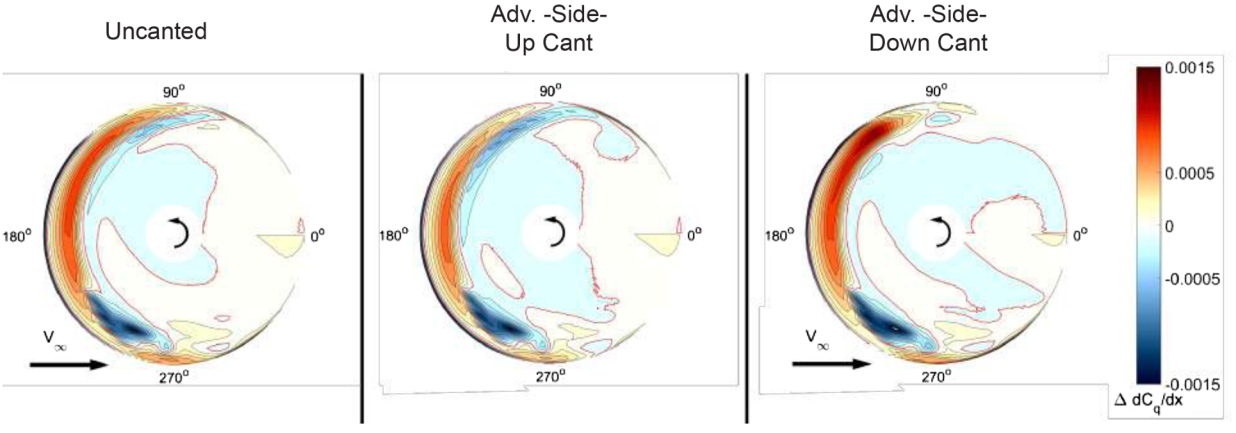

Fig. 14 Sectional torque coefficient difference, $\Delta dC_q/dx$ (aft rotor torque minus isolated rotor torque).

rotor produces 9.3% less lift than an uncanted isolated rotor. A canted inward aft rotor would see such a thrust loss (relative to an uncanted rotor) just due to canting, without consideration of rotor–rotor interactional aerodynamics.

Similarly, Fig. 17 presents the difference between thrust generated by a nose-up isolated rotor, and that generated by an uncanted isolated rotor. Here, a component of freestream acts upward on the rotor disk. The upwash through the rotor disk leads to an increase in thrust, as indicated by the white, yellow, and orange regions in Fig. 17. Integrated over the disk, a 6.6% lift increase is observed for a nose-up rotor. A canted outward aft rotor would see such a thrust gain (relative to an uncanted rotor) just due to canting, without consideration of rotor–rotor interactional aerodynamics.

Longitudinal canting of an isolated rotor also influences the torque. Figure 18 shows the difference in torque between an isolated nose-down rotor, and an isolated uncanted rotor. Although downwash over the rotor disk would be expected to increase torque due to a rearward tilt of the sectional lift vector, the reduction in rotor thrust (without adjustment of RPM or pitch) largely negates the expected increase. Figure 19 shows the difference in torque between an isolated nose-up rotor and an isolated uncanted rotor. Upwash through the rotor disk generally reduces torque due to reduction in induced drag. Indeed, a reduction in drag is observed over much of the rotor disk.

On the nose-down rotor, a region of torque reduction is seen at approximately $\psi = 230°$, where BVI is observed on an isolated uncanted rotor. BVI is not present on the nose-down rotor, leading to a relative torque reduction. On the nose-up rotor, however, strong BVI is found due to the freestream velocity pushing blade tip vortices produced at the front of the disk back into the disk plane. Strong BVI at about $\psi = 210°$ is seen to produce a region of high torque.

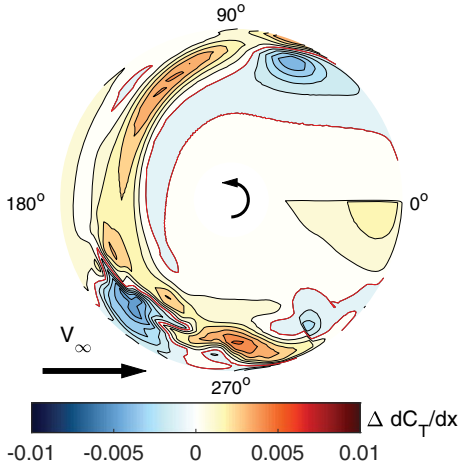

Fig. 17 Sectional thrust coefficient difference, $\Delta dC_t/dx$ (isolated nose-up thrust minus isolated uncanted rotor thrust).

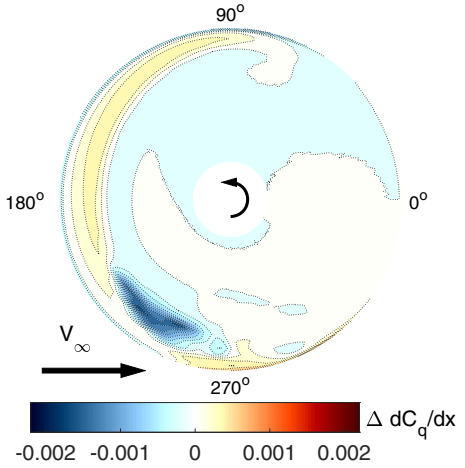

Fig. 18 Sectional torque coefficient difference, $\Delta dC_q/dx$ (isolated nose-down torque minus isolated uncanted rotor torque).

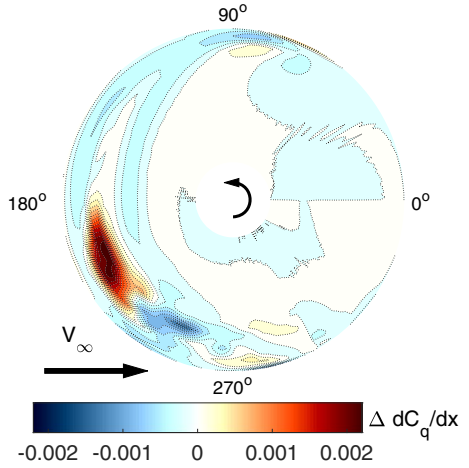

Fig. 19 Sectional torque coefficient difference, $\Delta dC_q/dx$ (isolated nose-up torque minus isolated uncanted rotor torque).

E. Longitudinal Cant Aerodynamics

Longitudinal cant changes the position of the aft rotor relative to the front rotor wake. Figure 20 shows the vertical velocity for isolated uncanted, nose-up and nose-down rotors over a slice cutting through the rotor hub as viewed from the left. The position of the front rotor, and the aft rotor disk (no aft rotor simulated), are also shown in pink. For each case, downwash is observed downstream of the front rotor, however, the position of the aft rotor modifies how much downwash it experiences. The uncanted aft rotor disk lies above the strongest downwash, but still intersects some darker blue toward the front. The front of the aft rotor in the canted inward case is seen to tilt down, causing it to intersect the region of strongest downwash. In contrast, the front of the aft rotor in the canted outward case is positioned up and consequently does not encounter very strong downwash.

The impact that rotor position has on the downwash observed by longitudinally canted aft rotors, as previewed in Fig. 20, can be observed over the whole aft rotor disk in Fig. 21. As with Fig. 12, a pink circle outlines the position occupied by an aft rotor disk. The interior of the pink circle is colored by velocity normal to the aft rotor plane. The uncanted aft rotor experiences stronger downwash on the front of the rotor disk, which dissipates toward the aft of the disk. The canted inward aft rotor observes yet stronger downwash near the front, as a result of its nose positioned closer to the front rotor wake. However, relatively little downwash is observed over the canted outward aft rotor disk, as its nose is positioned higher up and away from the front rotor wake.

F. Interaction Aerodynamic Impact of Longitudinal Cant on Thrust and Torque

The differences in downwash distribution over the longitudinally canted aft rotor disks influence their thrust generation and torque requirement due to the presence of the front rotor. Figure 22 presents the thrust difference between uncanted and longitudinally canted aft rotors, and isolated rotors in the same operating conditions: uncanted aft minus uncanted isolated (left), canted-in aft minus isolated nose down (middle), and canted-out aft minus isolated nose up (right). These comparisons identify how changes in longitudinal canting impact interactional aerodynamics, excluding changes brought about by changing the rotors' angle of attack. Due to its strong downwash over the front of the rotor disk, the canted-in aft rotor (middle) loses the most lift at the front. The lift loss is greater than that observed for an uncanted aft rotor (left). The canted-out aft rotor (right), however, observes relatively little downwash over the front of the disk, leading to a smaller lift loss overall.

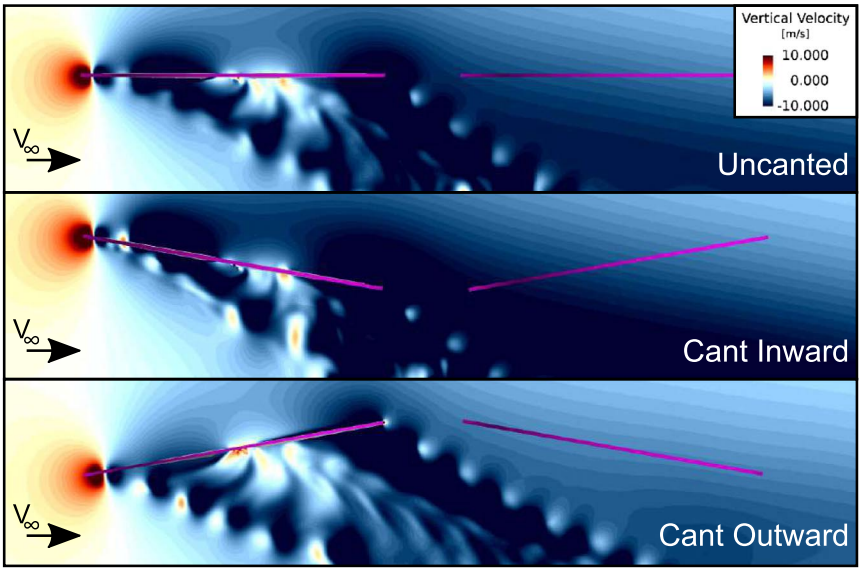

Fig. 20 Vertical velocity generated by isolated uncanted, nose-up, and nose-down rotors over a slice cutting through the rotor hub, as viewed from the side.

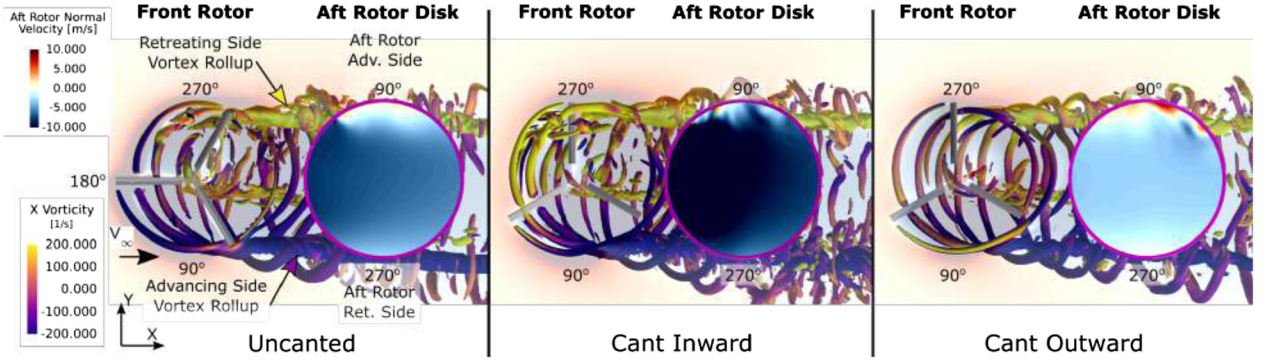

Fig. 21 Vertical velocity generated by isolated uncanted, nose-up, and nose-down rotors over the aft rotor disk location, as viewed from above. Isosurfaces of Q-criterion colored by vorticity in the downstream direction are also included.

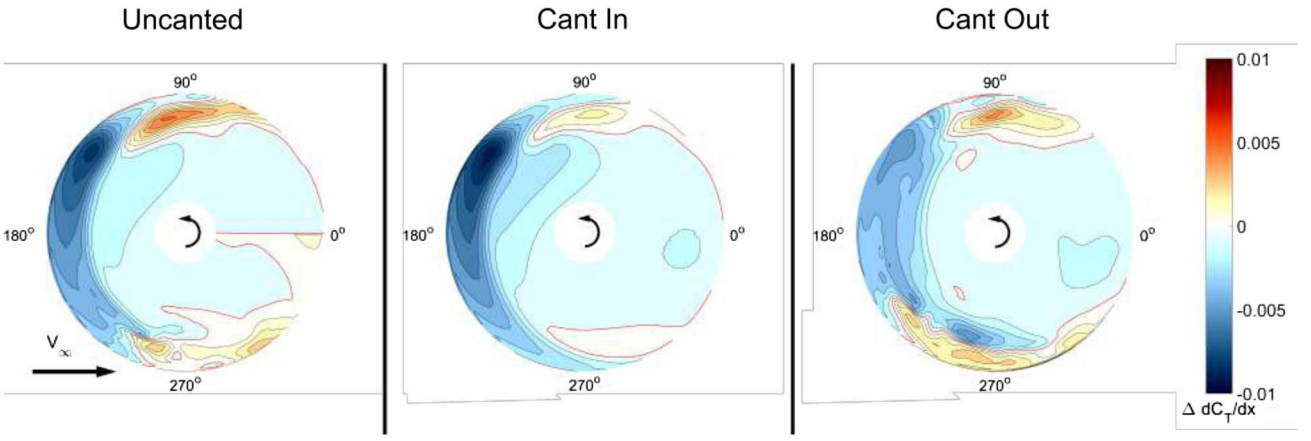

Fig. 22 Sectional thrust coefficient difference, $\Delta dC_t/dx$ (aft rotor thrust minus isolated rotor thrust).

As with thrust, differences in interactional aerodynamics also impact torque. Figure 23 shows the aft rotor torque difference between uncanted and longitudinally canted aft rotors, and their respective isolated rotor counterparts. Overall, downwash on the front of the disks tends to increase torque. The canted inward aft rotor is found to produce less of a torque increase on the front of the disk than the uncanted case. Despite the stronger downwash in this area, this could potentially be due to the substantial lift loss reducing induced drag. On the canted-out aft rotor, although a much smaller downwash is induced on the disk, equitable levels of torque increase to the uncanted case are observed. It is presumed that the relatively higher lift compared to the uncanted aft rotor produces greater induced drag.

No localized region of torque reduction is present on the cant in the case, as the isolated nose-down rotor does not experience significant BVI. In contrast, the canted-out aft rotor does show a region of torque reduction centered around $\psi = 225°$. Although the isolated nose- up

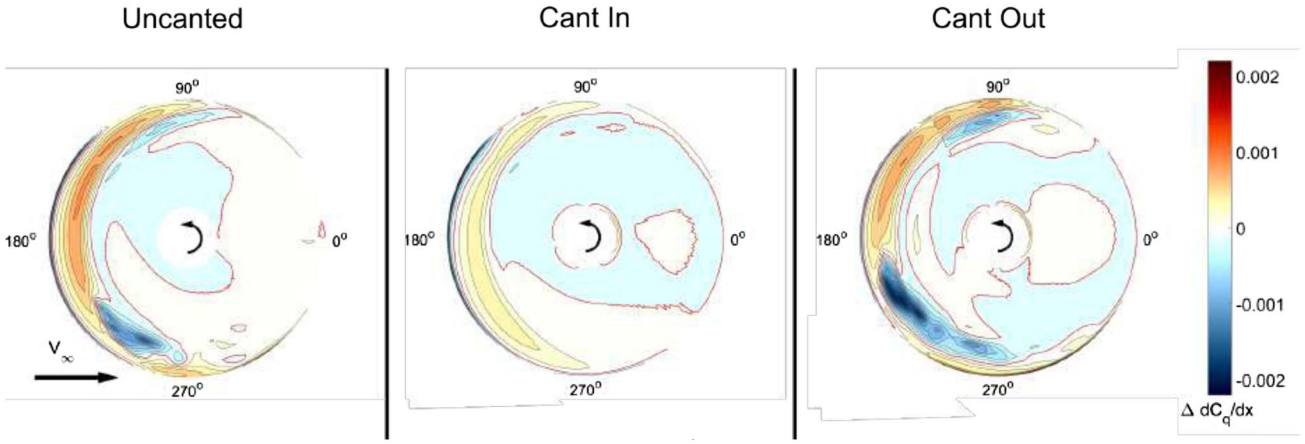

Fig. 23 Sectional torque coefficient difference, $\Delta dC_q/dx$ (aft rotor torque minus isolated rotor torque).

rotor produces BVI, the aft nose-up rotor in the cant-out configuration does not.

Table 2 summarizes the effects longitudinal canting has on thrust and torque due to changing the rotor's angle of attack, as well as due to interactional aerodynamic differences. Columns ΔT_α and ΔQ_α denote changes in thrust and torque due to changing the rotor's angle of attack. Columns ΔT_{aero} and ΔQ_{aero} represent changes in thrust and torque due purely to interactional aerodynamics by comparing them to longitudinally canted isolated rotors. Columns ΔT_{total} and ΔQ_{total} give total differences in thrust and torque between longitudinally canted aft rotors and an isolated uncanted rotor. The canted inward aft rotor loses some thrust due to angle of attack, however, a majority of its 26% thrust deficit is brought about by interactional aerodynamics, which are strongest due to proximity of the aft rotor to the front rotor wake. For the canted-out aft rotor, although some thrust improvement is gained by being angled nose- up, interactional aerodynamics still lead to a moderate 4% thrust deficit. Compared to the uncanted case, the low degree of interactional aerodynamics, coupled with the thrust improvement from upwash, leads to a relatively small deficit overall.

Integrated torque is also impacted by longitudinal canting, but to a much lesser degree. The canted-inward aft rotor has a net torque penalty of 2%, primarily due to interactional aerodynamics. The canted-outward aft rotor has a net torque reduction of under 1%, mainly due to the torque reduction associated with a rearward-tilted aft rotor.

G. Integrated Loads Comparison

Table 3 reports the changes in aft rotor thrust and hub moments (relative to the corresponding thrust and moments generated when the same rotor is operating in isolation) for all five cases in this study (uncanted, advancing-side-up and advancing-side-down lateral cant, and inward and outward lateral cant). Thrust is defined normal to the rotor disk (regardless of orientation), thus thrust difference indicates losses purely due to interactional aerodynamics. The aft rotor thrust deficit for the two laterally canted cases (advancing side up and advancing side down) is observed to be generally similar (18% and 16%, respectively), and only slightly higher than the thrust deficit for the uncanted aft rotor (15%). The two longitudinally canted cases, on the other hand, produce vastly different thrust deficits (11% for canted outward, and 21% for canted inward). Clearly, the canted-outward configuration results in the smallest interactional aerodynamic penalty on aft rotor thrust generation compared to the uncanted configuration, whereas the canted-inward configuration produces the largest penalty. The uncanted and advancing-side-down aft rotors require almost 7% more torque than an isolated rotor, whereas the advancing-side-up and longitudinally canted systems require less than 3% more torque than their isolated counterparts.

Table 2 Longitudinal cant thrust and torque breakdown for aft rotors

Configuration	ΔT_α	ΔT_{aero}	ΔT_{total}	ΔQ_α	ΔQ_{aero}	ΔQ_{total}
Uncanted	0.0%	−14.8%	−14.8%	0.0%	4.4%	4.4%
Cant Inward	−5.5%	−21.2%	−25.6%	−0.5%	2.7%	2.2%
Cant Outward	6.6%	−11.2%	−4.1%	−2.2%	1.6%	−0.7%

Table 3 Integrated thrust and torque difference between canted aft rotors and corresponding isolated rotors operating in the same operating conditions

Case	Thrust	Torque	Roll moment	Pitch moment
Uncanted	−14.8%	6.9%	−9.6%	−63.9%
Adv. Side Up	−17.5%	1.8%	28.1%	−61.3%
Adv. Side Down	−16.0%	7.0%	−37.7%	−55.1%
Canted Inward	−21.2%	2.7%	−11.0%	−94.1%
Canted Outward	−11.2%	1.6%	3.1%	−18.9%

For the uncanted and longitudinally canted rotors, because there was no dramatic lateral skew of the aft rotor lift deficit, the change in roll moment (relative to the rotor operating in isolation) is small and is observed to be in the 3–11% range. Lateral canting, on the other hand, skews the aft rotor lift deficit to the advancing or retreating side (Fig. 13) to produce much larger changes in roll moment (28–38%) than those observed for the uncanted and longitudinally canted cases. For the advancing-side-up lateral cant, the lift deficit skews to the retreating side to produce a roll-left moment change relative to the rotor operating in isolation. Conversely, for the advancing-side-down cant, the lift deficit skews to the advancing side, to instead produce a roll-right moment change.

With the aft rotor lift deficit always occurring at the front of the disk, this results in a net nose-down moment change for all five cases (relative to rotors operating in isolation). Because the uncanted and laterally canted configurations generally experience similar aft rotor lift deficits, the net nose-down pitching moments are also comparable (55–64%). On the other hand, with vastly differing lift deficits observed for the longitudinally canted cases, the changes in pitching moments show a wide variation as well. For the inward cant, where the aft rotor had the largest lift deficit, the change in pitching moment is as high as 94%. For the outward cant, where the aft rotor had the most modest lift deficit, the change in pitching moment is only 19%.

IV. Conclusions

This study investigates the impact of lateral and longitudinal rotor canting on interactional aerodynamics for two counter-rotating rotors positioned in-line with the flow. The computational fluid dynamics code AcuSolve, with detached eddy simulation, was used to simulate airflow through the system. The sliding mesh method was used to simulate blade motion by interfacing two rotating volumes (one for each rotor) within a nonrotating volume. The simulations were

performed for 5.5-ft-diameter, three-bladed rotors with uniform planform and linearly twisted blades spinning at 1600 RPM, corresponding to a 5 lb/ft^2 target disk loading. In all, five two-rotor cases were simulated: uncanted, 10° lateral cant with advancing sides up, 10° lateral cant with advancing sides down, 10° longitudinal cant inward, and 10° longitudinal cant outward. Additional isolated rotor cases were also simulated, corresponding to each of the aft rotors' operating conditions. These isolated rotor simulations were used to quantify the thrust and moment differences between them and the aft rotors experiencing aerodynamic interactions due to the front rotor. Through these simulations, the following observations were made:

1) Regardless of the cant orientation, the front rotor's wake induces downwash on the aft rotor, leading to a decrease in thrust generation. Downwash (and as a result, lift deficit) is most predominantly observed on the front of the aft rotor disk due to downward front rotor wake convection with longitudinal distance. Lift deficit on the front of the rotor disk leads to a nose-down pitching moment relative to a rotor in isolation.

2) An uncanted aft rotor is positioned above the front rotor's advancing and retreating side rollup vortices, and avoids the strongest downwash generated by the front rotor. However, when the aft rotor is laterally canted with advancing side up, its retreating side moves closer to the front rotor's advancing side rollup vortex where downwash is strong. Stronger downwash on the retreating side of the disk skews the lift deficit on the front of the rotor toward the retreating side, which also results in a roll-left moment relative to the isolated rotor. In contrast, when the aft rotor is laterally canted with advancing side *down*, it is the advancing side that moves closer to the front rotor's retreating side rollup vortex. In this case, it is the advancing side that observes the greatest downwash. This skews the lift deficit toward the advancing side, which results in a roll-right moment relative to the isolated rotor.

3) Longitudinally canting the rotors inward results in the front of the nose-down aft rotor being positioned closer to the front rotor wake, within strong downwash. Strong downwash over the front of the rotor disk leads to higher thrust deficits than those observed on an uncanted aft rotor. High thrust penalties on the front of the disk results in strong nose-down pitching moment relative to an isolated rotor. Longitudinally canting outward, however, positions the front of the nose-up aft rotor farther away from the front rotor wake. With the front of the aft rotor disk out of the strongest downwash, the thrust penalties in this region are reduced. This further reduces the nose-down moment relative to an isolated rotor.

4) Thrust penalties for uncanted and laterally canted aft rotors are moderate, ranging from 15% to 18%. Moderate thrust penalties correspond to moderate changes in pitching moment (55–64%). Longitudinally canting the rotors, however, dramatically changes the thrust penalty. Canting inward increases the lift deficit to as high as 21% with a 95% increase in nose-down pitching moment. Canting outward results in a lift deficit of 11% and a 19% increase in nose-down pitching moment. Overall, changes in torque are significantly lower than changes in lift and pitching moment. The change in rolling moment for uncanted and longitudinally canted rotors is moderate. However, laterally canted rotors modify the roll moment by up to 28–38%.

Acknowledgments

We would like to acknowledge the support of Boeing for this project, and the technical input of Boeing engineers David Mason, Ted Meadowcroft, Roger Lacy, Rachel Nelson, and Mori Mani.

References

[1] Yoon, S., Pulliam, T. H., and Chaderjian, N. M., "Simulations of XV-15 Rotor Flows in Hover Using Overflow," *Proceedings of the AHS 5th Aeromechanics Specialists Conference*, AHS Paper sm_aeromech_2014_042, San Francisco, CA, Jan. 2014.

[2] Yoon, S., Lee, H. C., and Pulliam, T. H., "Computational Analysis of Multi-Rotor Flows," *54th AIAA Aerospace Sciences Meeting*, AIAA Paper 2016-0812, Jan. 2016. https://doi.org/10.2514/6.2016-0812

[3] Yoon, S., Diaz, P. V., Boyd, D. D. Jr, Chan, W. M., and Theodore, C. R., "Computational Aerodynamic Modeling of Small Quadcopter Vehicles," *73rd Annual Forum of the American Helicopter Society*, AHS Paper 73-2017-0015, 2017.

[4] Ventura Diaz, P., and Yoon, S., "High-Fidelity Computational Aerodynamics of Multi-Rotor Unmanned Aerial Vehicles," *AIAA SciTech Forum*, AIAA Paper 2018-1266, 2018. https://doi.org/10.2514/6.2018-1266

[5] Misiorowski, M., Gandhi, F., and Oberai, A. A., "Computational Study on Rotor Interactional Effects for a Quadcopter in Edgewise Flight," *AIAA Journal*, Vol. 57, No. 12, 2019, pp. 5309–5319. https://doi.org/10.2514/1.J058369

[6] Duivenvoorden, R., Voskuijl, M., Morée, L., de Vries, J., and van der Veen, F., "Numerical and Experimental Investigation into the Aerodynamic Benefits of Rotorcraft Formation Flight," *76th Annual Forum of the Vertical Flight Society*, VFS Paper 76-2020-0106-Voskuijl, Virtual, 2020.

[7] Healy, R., Misiorowski, M., and Gandhi, F., "A Systematic CFD-Based Examination of Rotor-Rotor Separation Effects on Interactional Aerodynamics for Large eVTOL Aircraft," *75th Annual Forum of the Vertical Flight Society*, VFS Paper 75_2019_0379_Healy, Philadelphia, 2019.

[8] Russell, C., and Conley, S., "The Multirotor Test Bed—A New NASA Test Capability for Advanced VTOL Rotorcraft Configurations," *76th Annual Forum of the Vertical Flight Society*, VFS Paper 76-2020-0356-Russell, Virtual, 2020.

[9] Conley, S., Russell, C., Kallstrom, K., Koning, W., and Romander, E., "Comparing RotCFD Predictions of the Multirotor Test Bed with Experimental Results," *76th Annual Forum of the Vertical Flight Society*, VFS Paper 76-2020-0357-Conley, Virtual, 2020.

[10] Phillips, B., Hrishikeshavan, V., Yeo, D., and Chopra, I., "Experimental Evaluation of a Quadrotor Biplane with Variable Pitch Rotors," *73rd Annual Forum of the American Helicopter Society*, AHS Paper 73-2017-0326, Fort Worth, TX, 2017.

[11] Niemiec, R., and Gandhi, F., "Effect of Rotor Cant on Trim and Autonomous Flight Dynamics of a Quadcopter," *74th Annual Forum of the American Helicopter Society*, AHS Paper 74-2018-0178, Phoenix, 2018.

[12] Walter, A., McKay, M., Niemiec, R., Gandhi, F., and Ivler, C., "Handling Qualities Based Assessment of Scalability for Variable-RPM Electric Multi-Rotor Aircraft," *75th Annual Forum of the Vertical Flight Society*, VFS Paper 75_2019_0190_Walter, Philadelphia, 2019.

[13] Walter, A., McKay, M., Niemiec, R., Gandhi, F., and Ivler, C., "Hover Handling Qualities of Fixed-Pitch, Variable-RPM Quadcopters with Increasing Rotor Diameter," *76th Annual Forum of the Vertical Flight Society*, VFS Paper, Virtual, 2020.

[14] Bahr, M., McKay, M., Niemiec, R., and Gandhi, F., "Handling Qualities Assessment of Large Variable-RPM Multi-Rotor Aircraft for Urban Air Mobility," *76th Annual Forum of the Vertical Flight Society*, VFS Paper 76-2020-0126-Bahr, Virtual, 2020.

[15] Niemiec, R., Gandhi, F., Lopez, M. J. S., and Tischler, M. B., "System Identification and Handling Qualities Predictions of an eVTOL Urban Air Mobility Aircraft Using Modern Flight Control Methods," *76th Annual Forum of the Vertical Flight Society*, VFS Paper 76-2020-0007-Niemiec, Virtual, 2020.

[16] "AcuSolve Validation—NACA 0012 Airfoil," 2010, https://altairhyperworks.com/ResourceLibrary.aspx?keywords=validation\&altair_products=AcuSolve\&category [retrieved 19 Feb. 2014].

[17] Publications, V. F. S., "Aurora PAV eVTOL Model," June 2019, https://gallery.vtol.org/search/images/?q=aurora+pav [retrieved 28 May 2021].

[18] Niemiec, R., and Gandhi, F., "Development and Validation of the Rensselaer Multicopter Analysis Code (RMAC): A Physics-Based Low-Fidelity Modeling Tool," *75th Annual Forum of the Vertical Flight Society*, Paper 75_2019_0367_Niemiec, Philadelphia, PA, 2019.

[19] Corson, D., Jaiman, R., and Shakib, F., "Industrial Application of RANS Modelling: Capabilities and Needs," *International Journal of Computational Fluid Dynamics*, Vol. 23, No. 4, 2009, pp. 337–347. https://doi.org/10.1080/10618560902776810

[20] Misiorowski, M. P., Gandhi, F. S., and Oberai, A. A., "Computational Study of Diffuser Length on Ducted Rotor Performance in Edgewise Flight," *AIAA Journal*, Vol. 57, No. 2, 2019, pp. 796–808. https://doi.org/10.2514/1.J057228

[21] Misiorowski, M. P., Gandhi, F. S., and Oberai, A. A., "Computational Analysis and Flow Physics of a Ducted Rotor in Edgewise Flight," *Journal of the American Helicopter Society*, Vol. 64, No. 4, 2019, pp. 1–14. https://doi.org/10.4050/JAHS.64.042004

[22] Jansen, K., Whiting, C., and Hulbert, G., "A Generalized—Method for Integrating the Filtered Navier–Stokes Equations with a Stabilized

Finite Element Method," *Computer Methods in Applied Mechanics and Engineering*, Vol. 190, Nos. 3–4, 2000, pp. 305–319. https://doi.org/10.1016/S0045-7825(00)00203-6

[23] Brooks, A. N., and Hughes, T. J. R., "Streamline Upwind/Petrov-Galerkin Formulations for Convection Dominated Flows with Particular Emphasis on the Incompressible Navier-Stokes Equations," *Computer Methods in Applied Mechanics and Engineering*, Vol. 32, Nos. 1–3, 1982, pp. 199–259. https://doi.org/10.1016/0045-7825(82)90071-8

[24] Misiorowski, M., Gandhi, F., and Oberai, A. A., "Computational Study on Rotor Interactional Effects for a Quadcopter in Edgewise Flight," *AIAA Journal*, Vol. 57, No. 12, 2019, pp. 5309–5319. https://doi.org/10.2514/1.J058369

[25] Niemiec, R., "Development and Application of a Medium-Fidelity Analysis Code for Multicopter Aerodynamics and Flight Mechanics," Ph.D. Thesis, Rensselaer Polytechnic Inst., Troy, NY, Aug. 2018.

A. R. Jones
Associate Editor